Materials Today Bio 34 (2025) 102189

Contents lists available at ScienceDirect

Materials Today Bio

journal homepage: www.journals.elsevier.com/materials-today-bio

Silk protein discoidal microparticles for site-specific delivery of docetaxel in metastatic lung cancer

Hyeyoun Cho [a,1], Sanghyo Park [a,1], Jun Young Park [b], Yoonho Hwang [a], Won Jun Kang [b], Jaehong Key [a,*]

[a] Department of Biomedical Engineering, Yonsei University, Wonju, 26493, Republic of Korea
[b] Department of Nuclear Medicine, Severance Hospital, Yonsei University College of Medicine, 50-1 Yonsei-ro, Seodaemun-gu, Seoul, 03722, Republic of Korea

ARTICLE INFO

Keywords:
Non-small cell lung cancer
Silk protein
Discoidal silk protein particles
Docetaxel
Drug delivery system

ABSTRACT

Silk proteins, such as silk sericin (SS) and silk fibroin (SF), have been shown to exhibit excellent biocompatibility, biodegradability, and low immunogenicity as drug delivery carriers. SS possesses antioxidant and anticancer adjuvant properties, whereas SF provides mechanical strength and structural stability, marking them as optimal materials for drug delivery systems. In this study, 3 μm discoidal silk protein particles (DSPs) based on silk sericin/silk fibroin (SS/SF) composites were developed for the loading of docetaxel (DTX). A comprehensive analysis was conducted to assess the morphological characteristics, particle size, zeta potential, drug loading content, and colloidal stability of the particles. *In vitro* studies utilizing human-derived non-small cell lung cancer (A549) and mouse-derived squamous cell carcinoma (SCC7) cell lines revealed that DTX-SS/SF-DSPs exhibited superior anticancer activity compared to both free DTX and DTX-SF-DSPs. *In vivo* biodistribution studies revealed that DTX-SS/SF-DSPs effectively accumulated in the lungs, with minimal accumulation in non-target organs, including the liver and kidneys. Anticancer efficacy evaluations showed a significant reduction in the number of tumor nodules and improvement in survival rates. Furthermore, histopathological analysis confirmed reduced inflammatory responses and the absence of major organ toxicity, demonstrating excellent biocompatibility. In conclusion, SS/SF-DSPs are a promising drug delivery system that can improve the therapeutic efficacy of anticancer drugs with minimal side effects, which can present a new paradigm in lung cancer treatment.

1. Introduction

Lung cancer is one of the most fatal cancers worldwide [1–4]. Approximately 85 % of lung cancer is categorized as non-small cell lung cancer (NSCLC), and the remaining 15 % is small cell lung cancer (SCLC). NSCLC can be further divided into adenocarcinoma (40 %), squamous cell carcinoma (30 %), and large cell carcinoma (15 %) [5,6]. The treatment methods for NSCLC include surgery, chemotherapy, immunotherapy, and radiation therapy. Among those, chemotherapy is the main treatment for NSCLC, which is treated alone or in combination with radiotherapy or immunotherapy [7–9]. However, chemotherapeutic drugs have the disadvantage of lack of precision because they nonspecifically affect both cancer cells and normal cells [10].

Docetaxel (DTX) is a widely used anticancer chemotherapy agent for the treatment of lung cancer [11,12]. DTX inhibits cell division by stabilizing microtubule formation and causes cell death by preventing the complete division of cancer cells. However, DTX can cause serious side effects such as gastrointestinal symptoms (vomiting, nausea, diarrhea), musculoskeletal pain, hematopoietic disorders, and hair loss [13,14]. To reduce the adverse effects of chemotherapeutic drugs, various drug delivery systems have been exploited for cancer treatment [15]. Drug delivery systems are technologies that deliver therapeutic molecules to targeted body areas, either locally or systemically [16]. Drug delivery systems can reduce the distribution of drugs to non-target tissues and organs, thereby minimizing damage to normal tissues [17]. Additionally, drug delivery systems not only enhance the stability and absorption rate of drugs but also extend the duration of the presence of the drug in the body [18]. However, up to 70 % of the nano-sized drug delivery systems are isolated by Kupffer cells in the liver when administered *in vivo*. Therefore, nano-sized particles are less likely to be delivered to the lungs [19].

Recently, there has been a growing interest in the development of

* Corresponding author.
E-mail address: jkey@yonsei.ac.kr (J. Key).
[1] Authors contributed equally.

https://doi.org/10.1016/j.mtbio.2025.102189
Received 29 May 2025; Received in revised form 29 July 2025; Accepted 9 August 2025
Available online 9 August 2025

drug delivery systems made of materials derived from natural polymers. Natural polymers are biodegradable, biocompatible, and non-toxic, so drug delivery systems based on natural materials can be an effective alternative in various medical fields, including cancer treatment [20].

Among natural polymers, silk protein (SP) produced by *Bombyx mori* has been extensively studied in biomedicine, cosmetics, and structural materials. In biomedicine, fibroin and sericin have been widely applied in tissue engineering, wound healing, and drug delivery systems due to their biocompatibility and low immunogenicity [20,21]. In cosmetics, sericin is valued for its moisturizing, antioxidant, and anti-inflammatory properties, contributing to skincare and anti-aging formulations [22]. Structurally, silk fibroin exhibits high mechanical strength and has been processed into hydrogels, films, sponges, and fibers for use in biomedical devices [23].

SP primarily comprises two structural proteins: silk fibroin (SF; 70–80 %) and silk sericin (SS; 20–30 %) [24]. SF exhibits excellent mechanical properties, biocompatibility, controllable biodegradability, and low immunogenicity [25–27]. SS acts as an adhesive connecting two strands of SF and contains a large amount of the hydrophilic amino acids serine and glycine [21,28]. Studies have been reported that SS induces a mild inflammatory response, exhibits low antigenicity and immunogenicity with anti-inflammatory properties [29]. SS has also shown anticancer effects against various types of cancer cells by stimulating apoptosis [30–32].

Recent studies have reported the development of silk fibroin nanoparticles (SFNs) with tunable size, dispersity, and surface chemistry for improved anticancer drug delivery [33–35]. These nanoscale carriers have shown enhanced tumor targeting and therapeutic efficacy through precise formulation strategies. In contrast, our study introduces a micron-scale discoidal silk platform designed for passive lung targeting via capillary entrapment, offering distinct biodistribution and pharmacokinetic advantages over conventional SFNs.

In the present study, micro-sized silk sericin-silk fibroin-based discoidal silk protein particles (SS/SF-DSPs) were developed as a drug delivery system to improve the biocompatibility and efficacy of docetaxel. The docetaxel-loaded SS/SF-DSPs (DTX-SS/SF-DSPs) were characterized concerning morphology, size, zeta potential, and colloidal stability as well as their drug release profile. The toxicity and anticancer effects of DTX-SS/SF-DSPs were also investigated *in vitro* on SCC7 or A549 cells and *in vivo* lung metastasis mouse model. Results demonstrated that the DTX-SS/SF-DSPs significantly enhanced the anticancer properties of docetaxel with no signs of cytotoxicity.

2. Materials and methods

2.1. Reagents

All the materials were commercially available and used as received. SS and SF were extracted from *Bombyx mori* silk. Polydimethylsiloxane (PDMS; SYLGARD™ 184 Silicone Elastomer Kit) was purchased from Dow Corning (Midland, Michigan, USA). Poly(vinyl alcohol) (PVA; 80 % hydrolyzed, MW 9000–10,000 Da), dimethyl sulfoxide (DMSO), and 1,1,1,3,3,3-Hexafluoro-2-propanol (HFIP) were purchased from Sigma-Aldrich (St. Louis, Missouri, USA). Lithium bromide (LiBr), and docetaxel (DTX) were purchased from TCI (Tokyo, Japan). 1,1-Dioctadecyl-3,3,3,3′-tetramethylindotricarbocyanine iodide (DiR) was purchased from Cayman Chemicals (Ann Arbor, Michigan, USA). RPMI 1640 medium, fetal bovine serum (FBS) were purchased from Gibco, Thermo Fisher Scientific (Waltham, MA, USA). Antibiotic-Antimycotic (100X) was purchased from GenDEPOT (Barker, TX, USA). The Ez-Cytox cell viability assay kit was purchased from DoGenBio (Seoul, Korea). Human lung adenocarcinoma A549 cells and squamous cell carcinoma SCC7 cells were obtained from the American Tissue Culture Collection (ATCC).

2.2. Extraction of silk sericin

Silk sericin (SS) was extracted from silk cocoons of *Bombyx mori* silkworms using a previously described method with slight modification [36]. Briefly, the silk cocoons were cut into small pieces and mixed with deionized water (DW). The cocoon pieces were boiled at 100 °C for 30 min. After removing the supernatant impurities, the cocoon was heated at 120 °C for 90 min to extract sericin. Then, the undissolved fibrous silk fibroin and the dissolved sericin solution were separated using a nylon membrane (pore size: 100 μm). The separated liquid SS was freeze-dried in a freeze dryer for 3 days and stored in a refrigerator (Fig. S1).

2.3. Extraction of silk fibroin

Undissolved silk fibroin (SF) was spread on aluminum foil and dried overnight in a fume hood. Subsequently, the dried SF was dissolved in a 4 mL solution of 9.3 M LiBr per 1 g at 60 °C for 4 h. The 9.3 M LiBr solution was prepared using the following formula [23]:

$$Amount\ of\ LiBr = (86.85g/mol)(9.3mol/L)(1L/1000ml)(X)$$

Subsequent to the complete dissolution of the SF, the solution exhibited a translucent pumpkin color. Thereafter, the solution was placed in dialysis tubing (MWCO: 10 kD) and dialyzed against 2 L of distilled water while stirring for 3 days to remove LiBr [37]. Following this step, the desalted SF was freeze-dried for 3 days and stored in a refrigerator (Fig. S2).

2.4. Preparation of silk sericin/silk fibroin composites

The mixture of SS and SF was conducted at a ratio of 1:3 (w/w%), which is consistent with the composition of natural silk, which consists of 25 % SS and 75 % SF [38]. Freeze-dried SS (75 mg) and freeze-dried SF (225 mg) were dissolved in 4 mL of distilled water and subsequently mixed [39]. The resultant mixture was then subjected to a freeze-drying process for 3 days, thereby yielding the SS/SF composite.

2.5. Fabrication of DTX-SS/SF-DSPs

Discoidal silk protein particles (DSPs) loaded with DTX using a SS/SF composite (DTX-SS/SF-DSPs) were synthesized using a top-down fabrication approach. A silicon template with discoidal patterns 3 μm in diameter was prepared using electron beam lithography. A mixture of PDMS and elastomer (10:1, w/w %) was poured onto the silicon template and polymerized at 60 °C for 4 h to create a PDMS template. 48 g of PVA was dissolved in 800 mL of distilled water and then stirred at 60 °C for 2 h. The PVA solution was poured onto a polymerized PDMS template. After drying for a day, a PVA template with the same pattern as that of the silicon template was obtained.

The SS/SF composite was dissolved in 500 μL HFIP and heated at 60 °C for 24 h [40]. DTX was then added to the SS/SF solution and uniformly loaded over the PVA template. Thereafter, the PVA template was exposed to drying in a fume hood for 1 h, followed by immersion in 50 % (v/v) ethanol for 2 h. And then the PVA template was dissolved in 400 mL of distilled water for 2 h to obtain the microparticles. Undissolved PVAs and insoluble impurities were removed by nylon filters (pore size: 100 μm). The particles were collected using a membrane filter (pore size: 1.2 μm) under vacuum, effectively removing non-entrapped DTX. The particles were dispersed in DW and then collected by centrifugation at 3630 g for 1.5 min. The collected particles were freeze-dried and stored in a refrigerator.

2.6. Characterization and drug loading content

The particle size and zeta potential were measured using a Zetasizer (Nano ZS90, Malvern Panalytical, Malvern, UK). The particle morphology was observed using a scanning electron microscope (SEM)

(JSM-7600F, JEOL Ltd., Tokyo, Japan) and a confocal microscope (Carl Zeiss LSM710, Carl Zeiss AG, Oberkochen, Germany). The composition of the synthesized SS-SF was determined by proton nuclear magnetic resonance (NMR) spectroscopy.

To determine the drug loading content (LC%), DTX-SS/SF-DSPs were prepared by using different concentrations of docetaxel (10, 20, 30, and 40 mg). After dissolving the DTX-SS/SF-DSPs in DMSO at a concentration of 1 mg/mL, the quantity of docetaxel was determined by measuring the absorbance at a wavelength of 255 nm using a Synergy HTX multi-mode microplate reader (Biotek Instruments, Winooski, VT, USA). The content of docetaxel loaded onto SS/SF-DSPs was calculated based on the standard curve generated by measuring serial dilutions of docetaxel.

The drug loading content (LC%) was calculated by dissolving DTX-loaded particles in DMSO (1 mg/mL) and measuring the absorbance of encapsulated docetaxel at 255 nm using a UV–vis microplate reader. A standard curve of DTX in DMSO was used for quantification. Encapsulation efficiency (EE%) was not measured in this study. All experiments were conducted in quintuplicate (n = 5).

2.7. In vitro stability and drug release

The *in vitro* stability was assessed in phosphate-buffered saline (PBS) at 37 °C with varying pH conditions (pH5.4, pH7.4).

The particles were dispersed at 0.2 mg/mL, and the average hydrodynamic diameter was measured using a Zetasizer at predetermined time points over 10 days. The measured particle size at each time point was normalized to the initial size at 0 h (set as 100 %) to evaluate relative size changes.

The *in vitro* drug release profile was determined by using a dialysis capsule (MWCO: 10 kDa) to separate the docetaxel from the particles. 1 mg of DTX-SS/SF-DSPs was dispersed in 1 mL of PBS (pH5.4 or pH7.4) and transferred to a dialysis capsule, which was then reacted at a 37 °C. The release medium is removed at predetermined time intervals, and the drug concentration was determined using a microplate reader. All experiments were performed in quintuplicate (n = 5).

2.8. Cell culture and in vitro cytotoxicity

A549 and SCC7 cells were cultured in RPMI 1640 supplemented with 10 % FBS and 1 % Antibiotic-Antimycotic. The cells were maintained at 37 °C in a humid atmosphere containing 5 % CO_2. The cytotoxicity of DTX-SS/SF-DSPs was studied in A549 and SCC7 cells using the Ez-Cytox assay. DTX-SF-DSPs, DTX-SS/SF-DSPs, and docetaxel were adjusted to final concentrations of 0.03, 0.06, 0.13, 0.25, 0.5, and 1 mg/mL concentrations by diluting with the growth medium. After 24 h, 10 μL of EZ-Cytox was added to each well, and the plates were incubated at 37 °C for 2 h. After incubation, plates were read at 450 nm using a multi-mode reader. After 2 h, absorbance was measured at 450 nm using a microplate reader. Cell viability at each concentration was calculated relative to the untreated control group, which was set at 100 %. All cell viability assays were performed in quintuplicate (n = 5).

2.9. Biodistribution

All animal housing and experimental procedures adhered to the relevant guidelines and regulations of the Institutional Animal Care and Use Committee of Yonsei University, Wonju (YWCI-202211-017-02). Murine lung metastasis tumor models were prepared by intravenous inoculation of 5×10^6 A549 and SCC7 cells into 5-week-old BALB/c nude male mice.

Although SCC7 is a murine cell line commonly used in syngeneic models with immunocompetent mice, BALB/c nude mice were used in this study to enable consistent comparison with the A549 human xenograft model and to minimize immunological variability. The feasibility of SCC7 tumor formation in immunodeficient mice has also been demonstrated in previous studies [41,42].

To visualize the distribution of particles, we fabricated DSPs using 1,1-dioctadecyl-3,3,3,3′-tetramethylindotricarbocyanine iodide (DiR), a fluorescent dye that can mimic the distribution of DTX [43].

One week after cell injection, free DiR, DiR-SF-DSPs, or DiR-SS/SF-DSPs were injected through the tail vein. The mice were sacrificed at 2 h, 24 h, or 72 h post-injection. The major organs and tissues, including lung, liver, spleen, kidney, and heart samples were collected and imaged using a FOBI imaging system (Cellgentek, South Korea). At each time point, five mice per group were analyzed (n = 5).

Fluorescence was quantitated to analyze the distribution of DiR-SS/SF-DSPs using NEO image software.

2.10. In vivo therapeutic efficacy and systemic safety evaluation

The *in vivo* antitumor efficacy evaluation was carried out in A549 and SCC7 lung metastatic tumor models in BALB/c nude mice. A549 and SCC7 lung metastatic tumor-bearing mice were randomly divided into 4 groups: (a) control, (b) free DTX, (c) DTX-SF-DSPs, (d) DTX-SS/SF-DSPs. On day 7 after the tumor cell injection, mice were injected via the tail vein with saline, free DTX, DTX-SF-DSPs, or DTX-SS/SF-DSPs every three days for a total of 9 times. The dose of DTX was administered 30 μg equal to the amount loaded on DTX-SF-DSPs and DTX-SS/SF-DSPs. After 34 days of A549 and SCC7 cell injection, the mice were sacrificed, and the lungs and tumors were isolated. The number of metastatic nodules on the lung surface was measured under a dissecting microscope. For survival analysis, the mice were monitored daily up to day 30 after tumor cell inoculation, and the survival rate was calculated using the Kaplan-Meier method. Body weight was also monitored daily during the treatment period as an indicator of systemic toxicity. Each treatment group consisted of five mice (n = 5).

2.11. Histopathological analysis

Dissected organs were fixed with 4 % paraformaldehyde for 24 h and then paraffin-embedded using standard procedures. Sections were cut at 5 μm, dewaxed using hydration and xylene, and stained with hematoxylin and eosin (H&E). The H&E-stained sections were observed under an inverted microscope (Olympus, Tokyo, Japan).

2.12. Statistical analysis

All data were expressed as mean ± standard deviation (SD). All experiments were conducted in quintuplicate (n = 5). One-way analysis of variance (ANOVA) or unpaired two-tailed Student's t-tests were used to establish statistical significance using SigmaPlot 12.0 (Systat Software, Inc., Chicago, IL, USA). Differences were considered statistically significant at $^*P < 0.05$, $^{**}P < 0.01$, $^{***}P < 0.005$, and $^{****}P < 0.001$.

3. Results

3.1. Fabrication and characterization of DSPs

We synthesized the discoidal silk protein-based microparticles using silk sericin and silk fibroin extracted from silk cocoons (Fig. 1A). SS was extracted by treating cocoons with distilled water at high temperatures.

Based on previous studies using similar autoclave-based extraction methods, the molecular weight of silk sericin was estimated to range from 20 to 200 kDa, while that of regenerated SF was approximately 350 kDa [44,45].

This extraction method is simple and environmentally friendly, requiring no chemical reagents such as acids, bases, or enzymes, which is particularly important in this study as the biological activity of sericin needs to be preserved [44,45].

SF can be prepared by the filtration of SS-extracted solution using a nanofiber membrane. DTX-SS/SF-DSPs were synthesized via a top-down

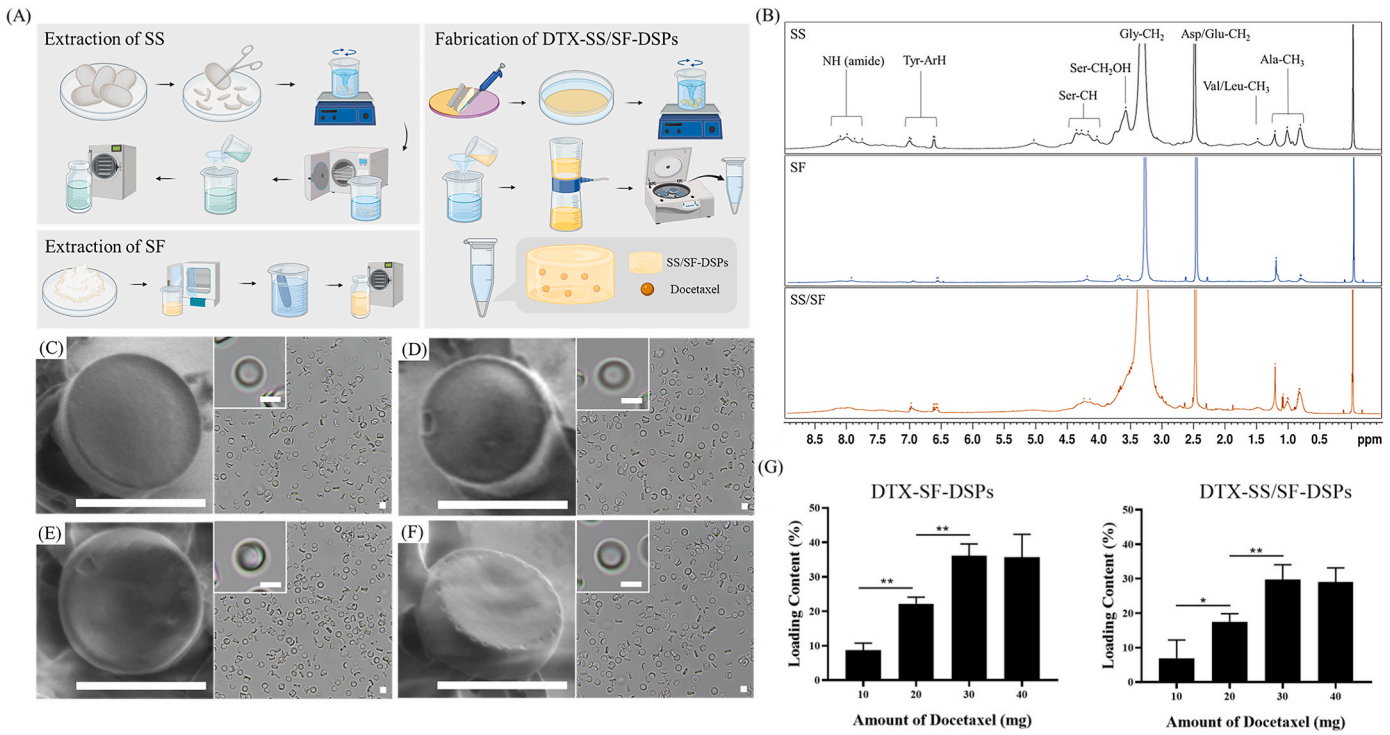

Fig. 1. Fabrication and morphological characterization of particles. (A) Schematic of the fabrication of docetaxel-loaded discoidal silk protein particles (DTX-DSPs). Silk sericin (SS) and silk fibroin (SF) proteins were extracted from cocoons of *Bombyx mori* silk worms. DTX-SS/SF-DSPs were produced via a top-down template-based fabrication technique, mixing DTX, SS, and SF in a single polymer paste. (B) ^{1}H nuclear magnetic resonance spectra of silk sericin (SS), silk fibroin (SF), and SS/SF composites, with all major peaks labeled according to their corresponding amino acid residues. Morphological characterization of discoidal silk protein particles (DSPs). Scanning electron microscopy (SEM) and confocal laser scanning microscopy (CLSM) images of (C) SF-DSPs, (D) SS/SF-DSPs, (E) DTX-SF-DSPs, and (F) DTX-SS/SF-DSPs. Scale bar: 2 μm. (G) Drug loading content of DTX-SF-DSPs and DTX-SS/SF-DSPs according to the quantity of docetaxel (DTX). Data are presented as mean ± SD (n = 5 per group). Statistical analysis was performed by Student's *t*-test, $^{*}p < 0.05$, $^{**}p < 0.01$.

template-based fabrication method using SS/SF composites.

In the ^{1}H NMR spectra, characteristic peaks corresponding to major amino acid residues in silk proteins—including Ala-CH_3 (~1.2 ppm), Val/Leu-CH_3 (~1.6 ppm), Asp/Glu-CH_2 (~2.6 ppm), Gly-CH_2 (~3.3 ppm), Ser-CH_2OH (~3.8 ppm), Tyr-ArH (~6.9 ppm), and amide-NH (~7.8 ppm)—were consistently observed in SS, SF, and SS/SF composite samples without significant chemical shift changes. These findings suggest that the SS and SF components were physically blended without forming new covalent bonds, indicating successful incorporation of both proteins in the composite formulation [46–48].

The morphology and size of the DSPs were determined using SEM and confocal microscopy.

During the initial fabrication trials, we found that particles composed solely of SS (SS-DSPs and DTX-SS-DSPs) could not be stably produced. Due to SS's strong water solubility and insufficient structural stability, the matrix disintegrated during the aqueous PVA removal step, making it impossible to recover intact particles. For this reason, SS-only groups were excluded from further experiments.

The SEM images showed that SF-DSPs, SS/SF-DSPs, DTX-SF-DSPs, and DTX-SS/SF-DSPs exhibited discoidal morphology with a uniform size (Fig. 1C–F). Average particle sizes of the DSPs are summarized in Table 1. The average sizes of the SF-DSPs and SS/SF-DSPs were 2.74 ± 0.07 μm and 2.77 ± 0.09 μm, respectively. The particle sizes of DTX-SF-DSPs and DTX-SS/SF-DSPs were not significantly changed after drug loading, implying that the intrinsic size of the DSPs was not considerably altered by the incorporation of DTX.

The size distribution of each particle group was further evaluated by dynamic light scattering (DLS), which showed narrow and unimodal intensity profiles consistent with the SEM-based measurements (Fig. S3).

DSPs were optimized with varying DTX loadings to maximize the drug content. As shown in Fig. 1G, the drug loading of DSPs increased linearly with increasing DTX concentration and reached the highest loading capacity at the DTX concentration of 30 mg. The maximum drug loading content for DTX-SF-DSPs was 36.16 ± 3.37 %, and for DTX-SS/SF-DSPs it reached 29.71 ± 4.34 %.

Table 1
Size, ζ-potential, drug loading content, and PDI of DSPs. Particle size, zeta potential, drug loading content, and polydispersity index (PDI) for SF-DSPs, SS/SF-DSPs, DTX-SF-DSPs, and DTX-SS/SF DSPs. Data are expressed as mean ± SD (n = 5 per group).

	Size (d.μm)	ζ-Potential (mV)	Loading content (%)	PDI
SF-DSPs	2.74 ± 0.07	−29.03 ± 0.53	–	0.162
SS/SF-DSPs	2.77 ± 0.09	−25.37 ± 0.55	–	0.105
DTX-SF-DSPs	2.80 ± 0.06	−33.80 ± 0.29	36.16 ± 3.37	0.084
DTX-SS/SF-DSPs	2.83 ± 0.09	−31.60 ± 0.29	29.02 ± 4.09	0.118

All experiments using DTX-loaded DSPs were conducted using particles fabricated with 30 mg of DTX, which corresponded to the formulation with the highest drug loading content.

Zeta potentials represent the repulsion between the particles in the dispersion. Values in the range of −20 to −40 mV indicated significant electrostatic repulsion between particles, which reduces aggregation and increases colloidal stability [29,30]. The zeta potentials of SF-DSPs and SS/SF-DSPs were −29.03 ± 0.53 mV and −25.37 ± 0.55 mV, respectively (Table 1). The zeta potential of DTX-DSPs exhibited a shift towards a negative charge in comparison to DSPs, attributable to the hydroxyl group of DTX [49]. These data indicated that DSPs are appropriate for the drug delivery purpose due to their high drug loading efficiency and stable colloidal form.

A polydispersity index (PDI) value lower than 0.1 indicates a

homogeneous size distribution of particles [50]. The PDI value of all DSPs was approximately 0.1, indicating that the size distribution of DSPs was narrow and uniform. PDI results were consistent with visual inspection of the CLSM image (Table 1).

3.2. In vitro stability and drug release

Polymer stability and drug release kinetics were evaluated at pH 5.4, reflecting the pH of the tumor microenvironment, and pH 7.4, reflecting the normal physiological environment of the lung [51].

The stability studies of DSPs showed that these particles reduced in size in a time-dependent manner (Fig. 2A). After 10 days, the average size of SF-DSPs decreased by 30 % at pH 7.4, whereas about 40 % of SS/SF-DSPs shrank within the same period. Moreover, the particle size of SF-DSPs was reduced by 50 %, and SS/SF-DSPs by 60 % at pH 5.4. There was no significant difference in stability before and after loading the DTX. This may be because the amino acid structure of SF becomes unstable in acidic environments [52].

At pH 5.4, 100 % release of DTX was observed on day 2 for SS/SF-DSPs, whereas 100 % release was observed on day 7 for SF-DSPs (Fig. 2B). At pH 7.4, SS-DSPs and SS/SF-DSPs exhibited relatively slower drug release compared to acidic pH. SF consisted of a highly organized β-sheet structure that contributes to mechanical strength and stability [53]. This structure of SF allowed it to remain stable under physiological conditions such as pH 7.4. However, in a weakly acidic environment such as pH 5.4, the hydrogen bonds and hydrophobic interactions within the β-sheet structure are weakened, causing the protein matrix to partially unfold and decreasing the stability [54]. In addition, SS/SF-DSPs prepared by mixing SS and SF would have further promoted drug release by reducing stability in an acidic environment due to the hydrophilic components of SS.

This rapid release behavior observed at pH 5.4, with complete drug release within two days, corresponds closely with the degradation pattern seen in Fig. 2A, where a significant reduction in SS/SF-DSPs particle count was noted. This suggests that the matrix disintegration induced by acidic pH is a key driver of enhanced drug diffusion. The presence of sericin—known for its hydrophilic nature and susceptibility to hydrolysis—likely played a major role in accelerating this process, as compared to SF alone. Similar findings have been reported in other sericin- and silk fibroin-based drug delivery systems, where rapid release under acidic conditions was observed [55,56].

This property of silk proteins may prevent the early release of drugs from DSPs by maintaining the stable structure of particles at neutral pH, but in the microenvironment of tumors exhibiting acidity, the particles

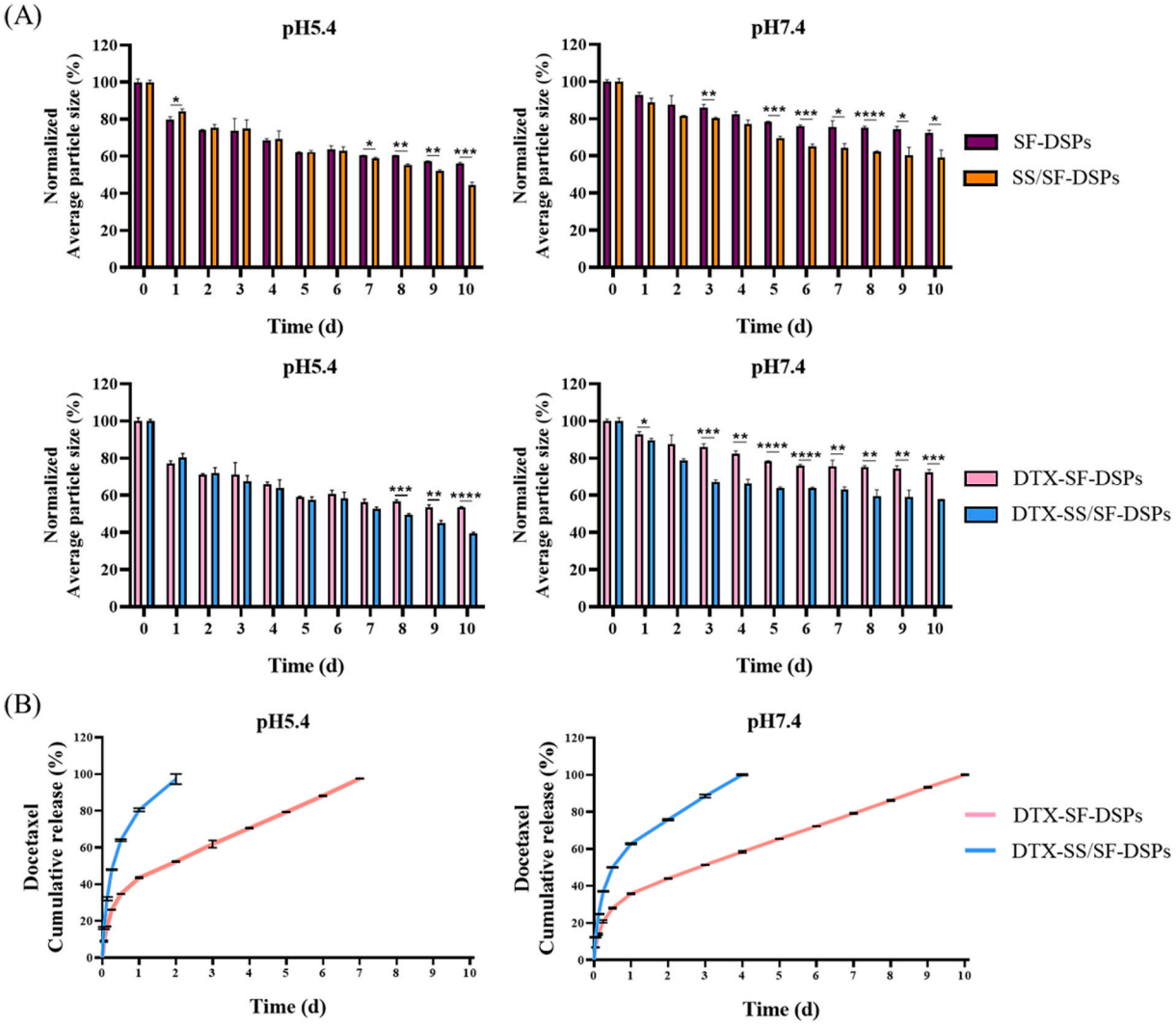

Fig. 2. pH-dependent stability and drug release profiles of discoidal silk protein particles (DSPs) over 10 d. (A) Normalized average particle size (%) of SF-DSPs, SS/SF-DSPs, DTX-SF-DSPs, and DTX-SS/SF-DSPs measured at pH 5.4 and pH 7.4 over time using a Zetasizer. Data are presented as mean ± SD (n = 5 per group). Statistically significant differences: $^{*}p < 0.05$, $^{**}p < 0.01$, $^{***}p < 0.005$, and $^{****}p < 0.001$. (B) Cumulative drug release profiles of DTX-SF DSPs and DTX-SS/SF DSPs at pH 5.4 and pH 7.4.

will decompose and release the drugs.

3.3. In vitro cytotoxicity

The cellular viability of DSPs and DTX-DSPs was investigated using A549 non-small cell lung cancer cells and SCC7 squamous cell carcinoma cells. As shown in Fig. 3A, DSPs exhibited a dose-dependent cytotoxic effect when incubated for 24 h at concentrations up to 1 mg/mL. The SS, SF, and Blank DSPs showed similar cytotoxicity in both A549 and SCC7 cells. Interestingly, the SS exhibited higher cytotoxicity than SF and SF-DSPs but showed similar toxicity to SS/SF-DSPs, indicating that SS further increases the cytotoxicity of particles. Sericin has shown anticancer properties by inducing sub-G1 phase cell cycle arrest and upregulation of the apoptotic signaling pathway in diverse tumor cells [31,57]. These findings suggest that sericin possesses prospective therapeutic applications for cancer treatment.

Cytotoxicity evaluation of DTX showed that the mortality of A549 cells exceeded 50 % when the concentration of free DTX was around 0.13 mg/mL (Fig. 3B). After 24 h of treatment with DTX, the viability of SCC7 cells was reduced to 50 % at concentration of 0.03 mg/mL, indicating that SCC7 cells were more sensitive to DTX than A549 cells.

This IC_{50} value (~0.13 mg/mL) for free docetaxel in SCC7 cells is consistent with previous studies reporting comparable cytotoxicity under similar experimental conditions. For instance, Oh et al. demonstrated that SCC7 cells treated with free docetaxel for 24 h exhibited viability patterns indicative of an IC_{50} in the range of 0.1–0.15 mg/mL, supporting the reliability of our findings under serum-containing conditions [58].

An increase in the concentration of DTX-SF-DSPs and DTX-SS/SF-DSPs led to a decrease in the viability of the A549 and SCC7 cells in a concentration-dependent manner. This result suggests that the more DTXs are delivered to the cells, the greater the cytotoxicity [30]. The inhibition rate of DTX-SS/SF-DSPs on the cell viability was significantly higher than that of the DTX-SF-DSPs. Cell viability assay results showed that a 0.25 mg/mL concentration of DTX-SF-DSPs reduced A549 cell viability to 70 % compared to the control, whereas DTX-SS/SF-DSPs reduced cell viability to 40 % at the same concentration. In SCC7 cells, at a concentration of 0.5 mg/mL, DTX-SF-DSPs reduced cell viability to 50 % compared to the control, but DTX-SS/SF-DSPs decreased to 35 %, and DTX-SS/SF-DSPs showed similar cytotoxicity to DTX. These cytotoxicity results would have been influenced by the drug release characteristics of particles because DTX-SS/SF-DSPs release drugs faster than DTX-SF-DSPs.

3.4. Ex-vivo biodistribution of DSPs

To evaluate the extent to which the DSPs can deliver DTX into tumors, the *ex vivo* distribution of DSPs in lungs and major organs was analyzed after DiR or DiR-labeled DSPs were injected into the SCC7 or A549-bearing mice. DiR was used instead of DTX because it can effectively mimic the biodistribution of DTX formulations [59]. As shown in Fig. 4, in mice that were injected with free DiR, significant fluorescence intensity was observed in the liver but very low in the lung at all time points. Nanoscale lipophilic DiR accumulates more in the liver than in other organs due to the large amount of blood supplied to the liver, and specialized cells such as Kupffer cells efficiently capture and maintain nanoparticles [51].

Mice injected with DiR-SF-DSPs and DiR-SS/SF-DSPs had a higher distribution of DSPs in the lungs compared to mice injected with free DiR. The fluorescence intensity of DiR-SF-DSPs and DiR-SS/SF-DSPs peaked in the lungs approximately 2 h after intravenous injection, whereas DSPs content slowly decreased over time. These results suggest that the particles accumulate quickly in the lungs within 2 h, reducing their distribution to other organs, thus having the potential to minimize adverse effects. The *in vivo* distribution of DSPs was similar between the two metastatic NSCLC models.

3.5. In vivo therapeutic efficacy and systemic safety of DSPs in lung metastasis models

The anticancer properties of DTX-SF-DSPs and DTX-SS/SF-DSPs were evaluated in lung metastatic models of A549 and SCC7 cells. The mice were randomly grouped and then intravenously injected with DTX-SF-DSPs and DTX-SS/SF-DSPs or free DTX at an identical dose to DTX-DSPs (Fig. 5A).

After DTX-DSPs treatment, the lungs of mice were harvested, photographed, and tumor nodules were calculated. The tumor nodules of the saline-treated group indicated the successful establishment of an *in vivo* lung metastatic model using A549 or SCC7 cells (Fig. 5B). Quantitative analysis showed that the average number of SCC7 cell lung

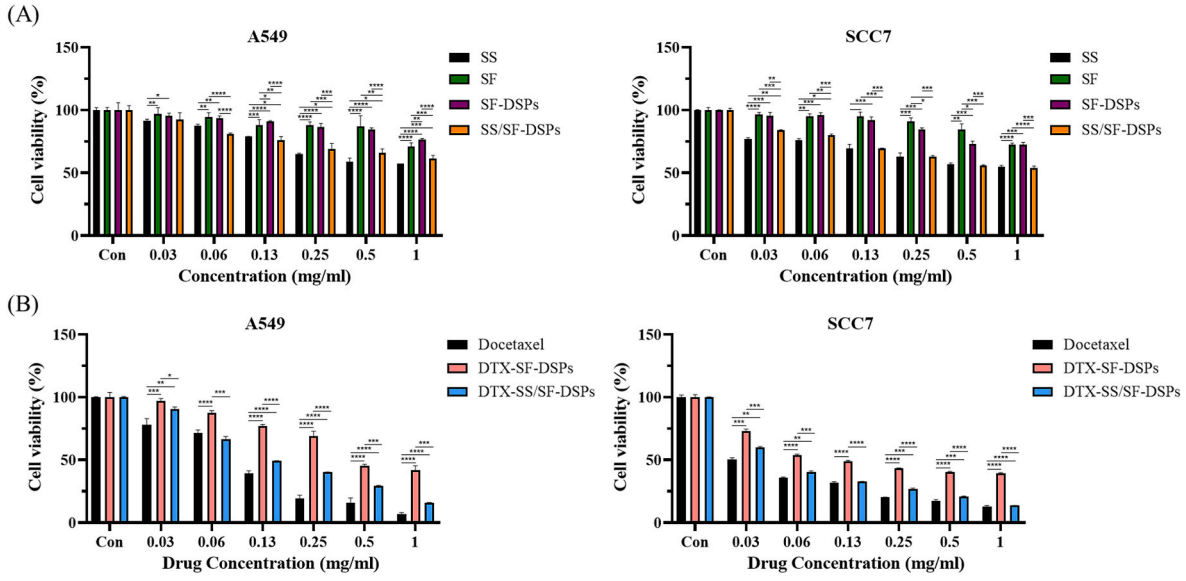

Fig. 3. *In vitro* cytotoxicity of DTX-DSPs on A549 and SCC7 cancer cell lines over time. (A) Cytotoxicity of SS, SF, SF DSPs, and SS/SF DSPs on A549 cells and SCC7. (B) Cytotoxicity of DTX and DTX-loaded DSPs. Data are presented as mean ± SD (n = 5 per group). Statistically significant differences: $^{*}p < 0.05$, $^{**}p < 0.01$, $^{***}p < 0.005$, and $^{****}p < 0.001$.

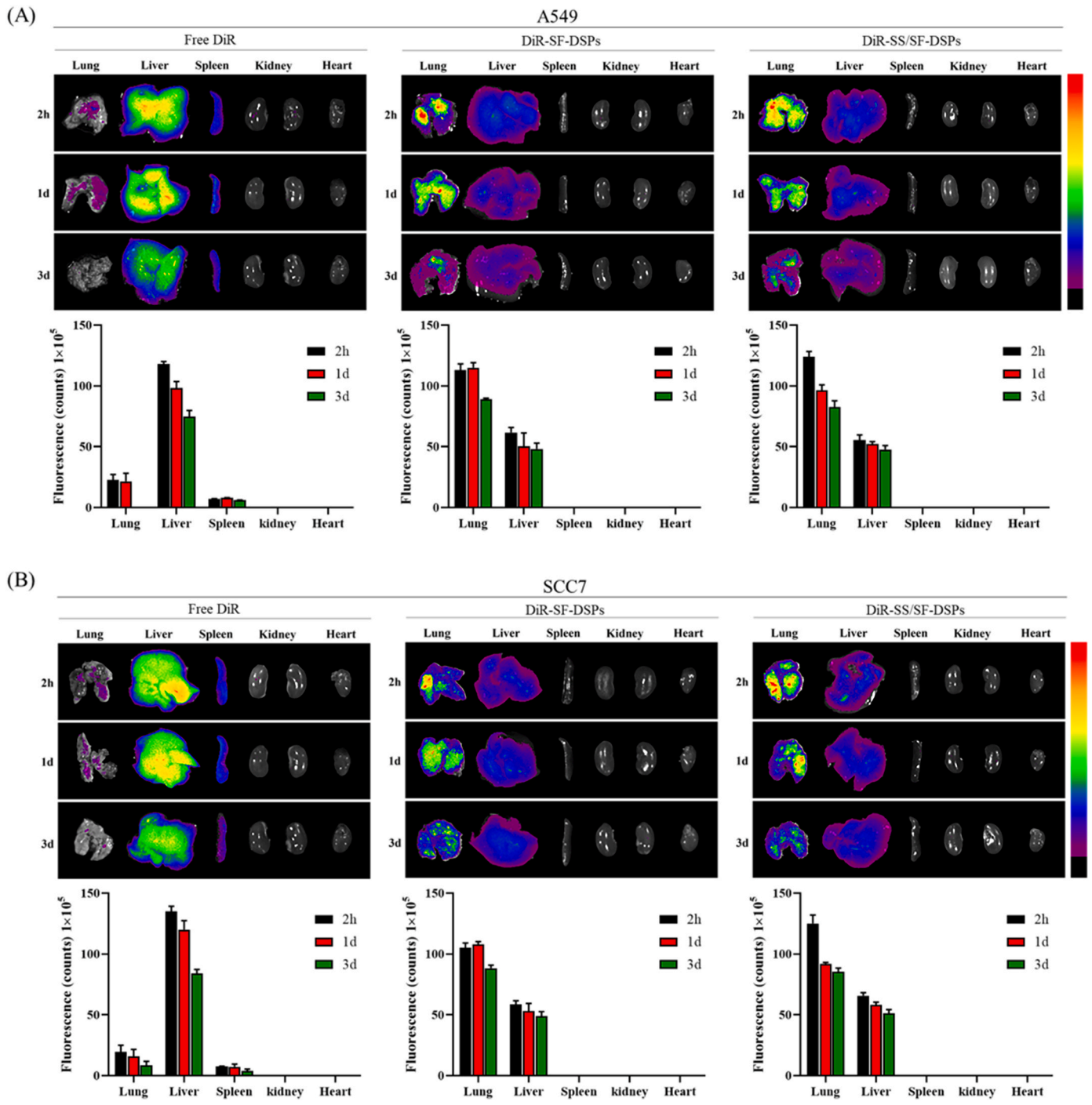

Fig. 4. *Ex vivo* biodistribution of discoidal silk protein particles (DSPs) in a lung metastatic model.
Ex vivo biodistribution of discoidal silk protein particles (DSPs) in a lung metastasis mouse model established by tail vein injection of (A) A549 and (B) SCC7 cells. Representative fluorescence images and semi-quantitative fluorescence intensity for *in vivo* distribution of free DiR, DiR-SF-DSPs, and DiR-SS/SF-DSPs were examined at 2 h, 24 h, and 72 h post-injection. Data are presented as the mean ± SD (n = 5 per group).

nodules in mice treated with DTX-SF-DSPs (11 ± 1 nodules) or DTX-SS/SF-DSPs (6 ± 1 nodules) was significantly lower compared with those treated with saline (75 ± 3 nodules) and even lower than in the DTX-treated group (21 ± 1 nodules) (Fig. 5C). Notably, the DTX-SS/SF-DSPs treatment group had a 92 % reduction in the mean number of SCC7 tumor nodules compared to the saline-treated group ($p < 0.001$). In the A549 lung metastatic model, the average number of tumor nodules was reduced by 85 % in the DTX-SS/SF-DSPs treatment group compared with the saline-treated group ($p < 0.001$). In the A549 and SCC7 lung metastasis models, the number of tumor nodules after treatment with DTX-SF-DSPs and DTX-SS/SF-DSPs was similar, respectively (Fig. 5C).

Next, we analyzed the survival rates to further evaluate the efficacy of the DTX-DSPs in the A549 and SCC7 lung metastasis models. The median survival of the SCC7 lung metastatic model was 12 days in the saline-treated group (Fig. 5D). However, the median survival of mice was increased by DTX treatment to 24 days and also by DTX-SF-DSPs treatment to 27 days. In the DTX-SS/SF-DSPs treatment group, 50 % of the mice survived to day 30. In the A549 lung metastatic model, the survival rates of mice in the DTX-SF-DSPs and DTX-SS/SF-DSPs

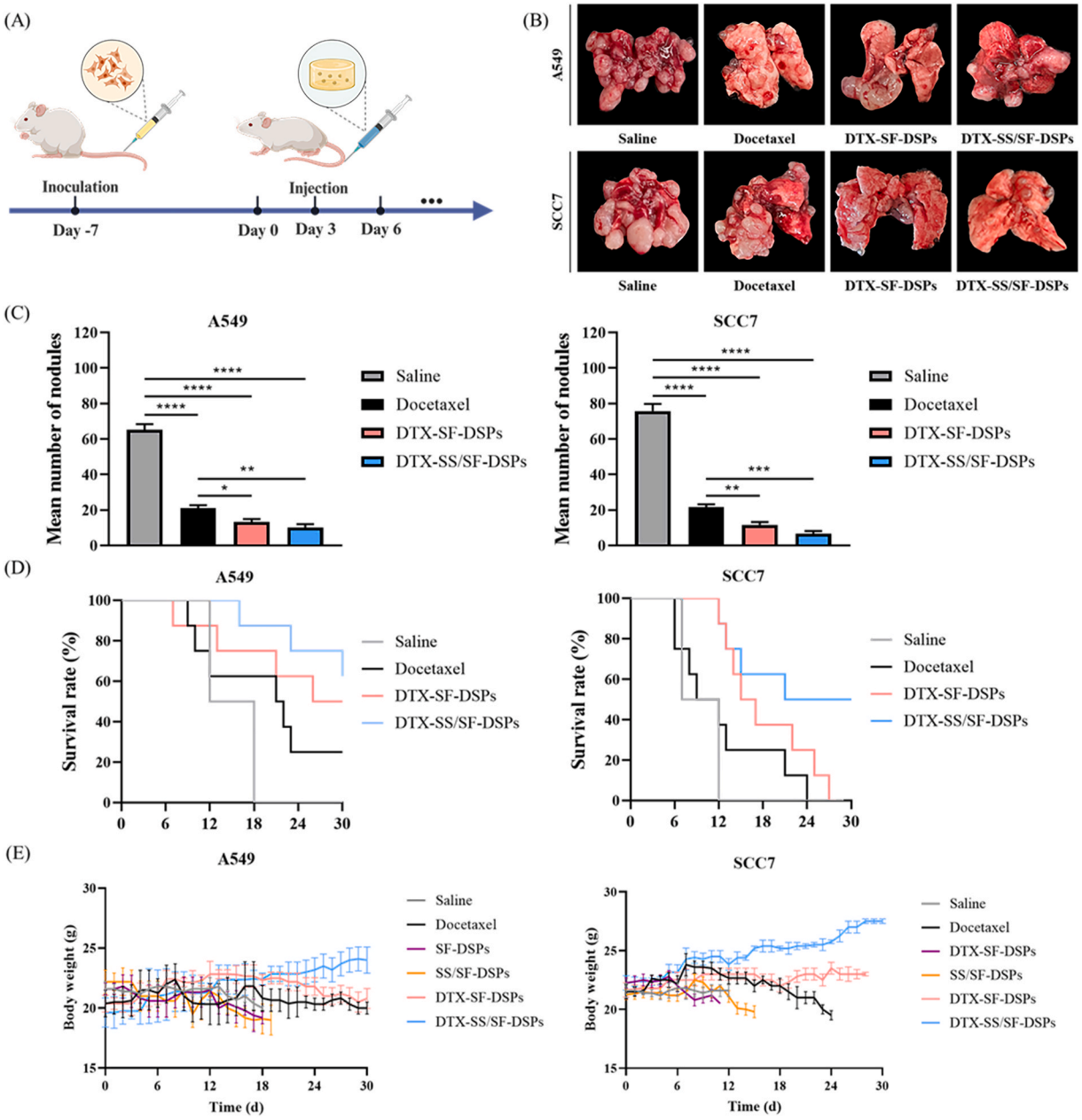

Fig. 5. In vivo therapeutic efficacy and systemic toxicity evaluation of DTX-DSPs in A549 and SCC7 lung metastatic models. (A) Schematic representation of the experimental timeline from tumor inoculation to treatment application. (B) Representative images of metastatic lung nodules harvested from mice that received saline or docetaxel (DTX) or DTX-SF-DSPs or DTX-SS/SF-DSPs. (C) Quantitative analysis of tumor nodules in the lungs of the murine model of lung metastases. (D) Kaplan-Meier survival analysis for the A549 and SCC7 lung metastatic model treated with DTX-DSPs, with 30 days week follow up. (E) Body weight changes in A549 and SCC7 tumor-bearing mice monitored throughout the treatment period to assess systemic toxicity. Data are given as the mean ± SD (n = 5 per group). Statistically significant differences: $^{*}p < 0.05$, $^{**}p < 0.01$, $^{***}p < 0.005$, and $^{****}p < 0.001$.

treatment groups were 50 % and 60 % at 30 days after treatment, respectively. The survival curves in the DTX-DSPs treatment groups showed that the A549 cell- and the SCC7 cell-induced model had different survival rates. Human and mouse cells have different physiological characteristics, which may affect the therapeutic efficacy of the cancer drug [40]. A549 cells are derived from human non-small cell lung cancer, whereas SCC7 cells are derived from mouse squamous cell carcinoma. Therefore, the treatment outcome may vary depending on the specific type of cancer. In addition, body weight changes were monitored throughout the treatment period as an indicator of systemic toxicity (Fig. 5E). No significant body weight loss was observed in any group, and mice treated with DTX-SS/SF-DSPs maintained the most stable body weight, indicating good systemic tolerability of the formulation.

3.6. *In vivo toxicity of DSPs*

The potential *in vivo* toxicity of the DTX-DSPs was evaluated by monitoring body weight and histopathological evaluation of the major organs. As shown in Fig. 5E, no significant body weight loss was observed over the course of the treatment, indicating that DTX-DSPs have low systemic toxicity under the given dosing regimen. Histopathological analysis of major organs, including the lungs, liver, spleen, kidneys, and heart, was performed to evaluate the tissue damage, inflammatory responses, and structural changes caused by the administration of DTX-SF-DSPs and DTX-SS/SF-DSPs. Representative H&E

staining images showing the tissue morphology and inflammatory response of each experimental group are shown in Fig. 6. In the saline-treated group, the alveolar space of the lung tissue decreased and inflammatory responses were observed. This result suggests that tissue damage was caused by the growth or inflammation of cancer cells. However, in the free DTX, DTX-SF-DSPs, and DTX-SS/SF-DSPs groups, alveolar space was maintained similar to that of normal mice, and a significant decrease in inflammation was observed when compared to the saline-treated group. Preservation of alveolar space and reduced inflammatory response in lung tissue are likely due to the combined effects of slow degradation of SF and anti-inflammatory properties of SS. No sign of toxicity was observed in the liver, spleen, kidney, and heart of mice in DTX-DSPs treatment group. Similar results were observed in both the A549 and SCC7 lung metastatic models, indicating that the DSPs do not cause toxicity in the non-target organs.

4. Discussion

Chemotherapy drugs including cisplatin, carboplatin, paclitaxel, docetaxel, gemcitabine, and vinorelbine are used as primary treatment options for non-small cell lung cancer (NSCLC) [60,61]. However, chemotherapy drugs can cause significant adverse effects. The adverse effects often worsen when the drug is systemically distributed throughout the body, so drugs should be delivered intensively only to the target tumors. Drug delivery systems are being utilized as important strategies to improve these problems. Recently, research on the development of drug delivery systems using natural products has been actively conducted, and silk proteins are especially attracting attention for their biocompatibility, biodegradability, and low toxicity [22]. Docetaxel has been widely used as a first- and second-line treatment for NSCLC, however owing to its systemic toxicity and short half-life in the body, the efficiency and biocompatibility of DTX need to be improved [62]. In the present study, we prepared micro-sized discoidal particles that were expected to achieve the lung-targeted delivery of DTX using silk proteins composed of silk sericin and silk fibroin. We compared the biocompatibility and therapeutic efficacy between SF-DSPs made from silk fibroin with strong mechanical strength and SS/SF-DSPs made by mixing SF with silk sericin having hydrophilicity and anticancer effects.

The successful formulation of SS/SF-DSPs was further supported by ^{1}H NMR spectroscopy, which revealed that the characteristic peaks of key amino acid residues—such as Ala, Val, Asp, Gly, Ser, and Tyr—appeared consistently across SS, SF, and SS/SF composite samples. The absence of significant chemical shift changes among them indicates that the proteins were physically blended rather than chemically modified. This implies that each protein component retained its intrinsic properties within a stable and uniform composite matrix [46–48].

In drug release tests, SS/SF-DSPs released docetaxel faster than SF-DSPs, and at acidic pH (pH 5.4), drugs were released faster than at neutral pH (pH 7.4). In a neutral environment, the β-sheet structure of SF remained stable, allowing the drug to be slowly released, minimizing toxicity to normal tissues.

In contrast, in an acidic environment, the destabilization of the silk matrix was facilitated by the hydrophilic and acid-labile nature of SS, while the β-sheet structure of SF was partially disrupted due to weakened hydrogen bonding and hydrophobic interactions, rather than disulfide bond cleavage [44,45].

This suggests that selective drug release can be induced in the acidic microenvironment of tumor cells, thereby enhancing the therapeutic efficacy of chemotherapy drugs.

Although the β-sheet content of silk fibroin is known to increase under acidic conditions, the faster drug release observed at pH 5.4 may be attributed to the higher solubility and acid-labile nature of sericin. In addition, mildly acidic conditions can weaken hydrogen bonding and promote hydrolytic cleavage within the silk matrix, which together may destabilize the structure and enhance water penetration. These effects likely outweigh the stabilizing influence of β-sheet formation, resulting

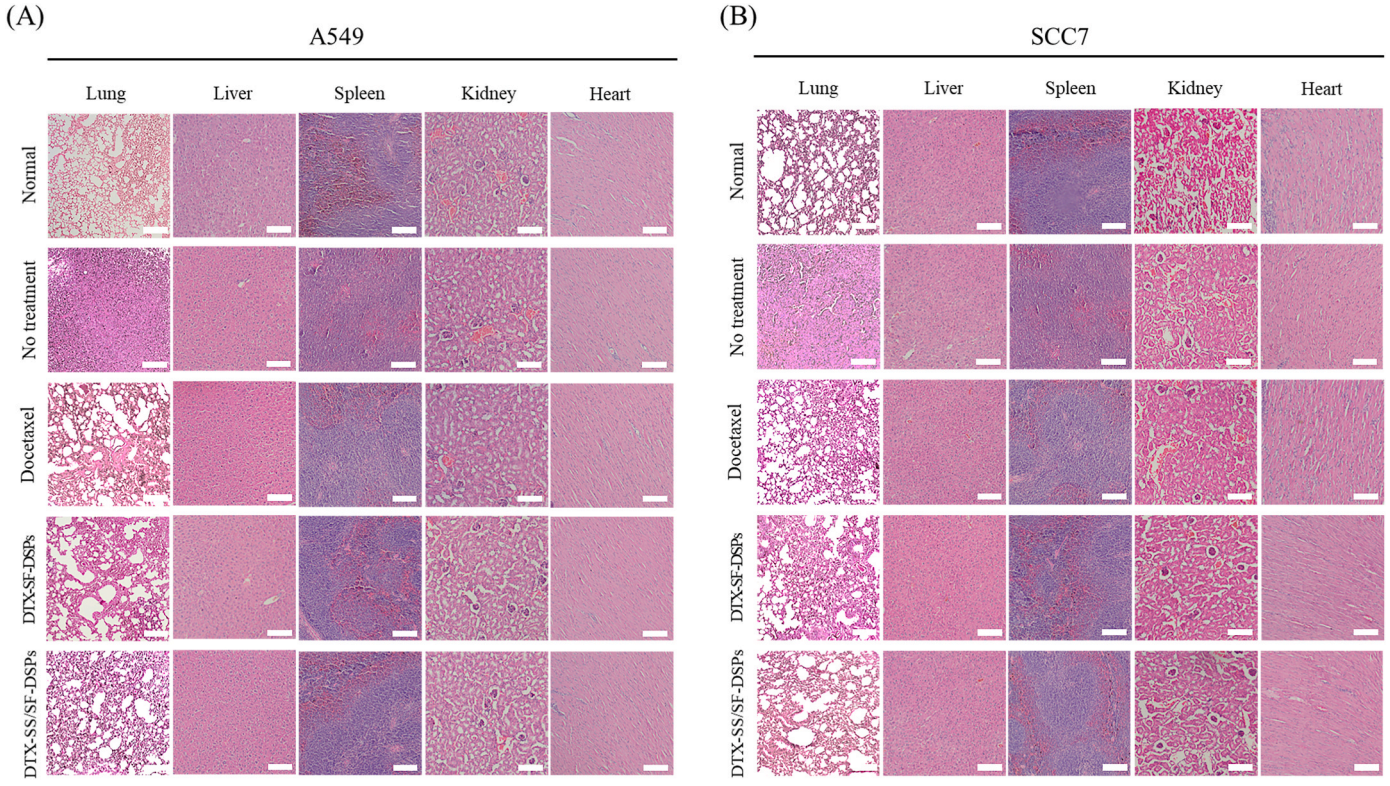

Fig. 6. Histopathological evaluation of major organs following treatment with docetaxel-loaded discoidal silk particles (DTX-DSPs) in lung metastasis models. Representative H&E-stained images of the lung, liver, spleen, kidney, and heart from (A) A549 and (B) SCC7 tumor-bearing mice after treatment with Saline, Docetaxel, DTX-SF-DSPs, and DTX-SS/SF-DSPs. Scale bars: 100 μm.

in accelerated release at low pH [63,64].

In the cytotoxicity evaluation, a similar decrease in cell viability was observed in both human-derived A549 cells and mouse-derived SCC7 cells, which demonstrates the reliability and reproducibility of DSPs.

In cytotoxicity assays, DTX-SS/SF-DSPs showed greater cancer cell killing than DTX-SF-DSPs or free DTX, suggesting that the incorporation of sericin enhanced the therapeutic potency of the particles through both physicochemical and biological mechanisms. The hydrophilic nature of sericin facilitated faster drug release in the acidic tumor microenvironment, as demonstrated by our pH-responsive release profile. This accelerated release likely enhanced docetaxel bioavailability at the tumor site and contributed to the improved cytotoxic outcomes.

Beyond drug delivery, sericin itself exhibited intrinsic anticancer activity that synergized with the effect of docetaxel. Specifically, sericin has been shown to elevate intracellular levels of reactive oxygen species (ROS), leading to mitochondrial membrane depolarization, cytochrome *c* release, and activation of the intrinsic apoptosis pathway through caspase-3 and caspase-9. Sericin also regulates the expression of key apoptotic proteins, upregulating pro-apoptotic Bax while downregulating anti-apoptotic Bcl-2. Furthermore, it induces cell cycle arrest in the G0/G1 or S-phase by modulating cell cycle-related proteins and inhibits cancer-associated signaling pathways such as PI3K/AKT/mTOR, MAPK, and NF-κB [31,65,66]. These mechanisms suggest that sericin not only functions as a structural matrix but actively contributes to tumor suppression at the molecular level.

Given their ~3 μm size and discoidal geometry, SS/SF-DSPs are unlikely to undergo internalization by non-phagocytic cancer cells. Instead, these particles preferentially adhere to the tumor cell surface and facilitate the localized release of docetaxel, enabling passive diffusion of the free drug into cells to elicit cytotoxic effects. This proposed mechanism is supported by our previous study employing DOX-loaded discoidal microparticles, which exhibited potent antitumor efficacy in the absence of cellular internalization, as well as earlier reports demonstrating that discoidal particles tend to marginate and interact with vascular walls rather than being endocytosed [67,68].

Notably, despite releasing only approximately 40 % of the loaded docetaxel within 24 h at pH 5.4, DTX-SS/SF-DSPs achieved cytotoxicity comparable to or greater than that of free DTX. This suggests that partial yet sustained exposure of cancer cells to the drug—combined with the intrinsic anticancer properties of sericin—was sufficient to induce strong therapeutic effects. In this context, the spatial and temporal delivery advantages of the microparticle system may outweigh the need for rapid or complete release within a short time frame [68–70].

In addition to these cellular-level mechanisms, recent studies have indicated that both docetaxel and sericin may influence oncogenic pathways critically involved in lung cancer progression and tumorigenesis. For instance, the PI3K/AKT/mTOR, MAPK, and NF-κB pathways regulate tumor initiation, proliferation, angiogenesis, and immune evasion in NSCLC [70–72]. Previous reports have shown that DTX and sericin can inhibit these pathways, suggesting that our DTX-SS/SF-DSPs may suppress tumor development by modulating these molecular signaling axes [71,73]. Based on these findings, we hypothesize that DTX-DSPs not only induce direct cytotoxicity but also intervene in molecular programs that drive tumor progression. To test this, we plan to conduct mechanistic studies such as western blotting, qPCR, and transcriptomic profiling to assess pathway inhibition in NSCLC cell lines (e.g., A549, H460). These investigations will help clarify how DTX-DSPs contribute to lung cancer suppression at a systems level.

Cell viability data showed that DTX-SS/SF-DSPs was more cytotoxic than the DTX-SF-DSPs, which would have synergized the microtubule-stabilizing effects of DTX and the anticancer effect of SS.

Biodistribution studies showed that fluorescent-loaded SS/SF-DSPs rapidly accumulated in the lung tissue, with low accumulation rates in non-target organs including liver and kidney. This is because the SS/SF-DSPs have a discoid shape and are 3 μm in size, which promotes lateral drift in the bloodstream, thereby increasing the accumulation efficiency in lung tissue [74].

In particular, discoidal particles around 3 μm in diameter are known to be passively retained in the lungs due to their physical entrapment within the narrow capillaries of the pulmonary circulation. Their size and shape promote margination toward the vessel walls, leading to enhanced accumulation in lung tissue following intravenous injection [68]. Furthermore, non-spherical particles with diameters of 3 μm or larger are phagocytosed less efficiently by hepatic Kupffer cells compared to smaller or spherical particles, owing to their unfavorable curvature for membrane wrapping and internalization [69]. In addition, previous studies from our group have validated the safety and lung-targeting efficacy of 3 μm discoidal particles following IV injection in various disease models, including pulmonary fibrosis and lung metastasis [42,67,74,75].

The anticancer efficacy and survival rate analysis revealed that the treatment of DTX-SS/SF-DSPs significantly reduced the number of metastatic tumor nodules and improved survival rate compared to free DTX and DTX-SF DSPs in the SCC7 and A549 lung metastasis models. Histopathological analysis revealed that the treatment of DTX-SS/SF-DSPs decreased the inflammation and maintenance of lung tissue structure compared to the saline-treated A549 and SCC7 lung metastasis models. No signs of toxicity were observed in non-target organs, indicating the excellent safety of DTX-DSPs. These results demonstrated that DSPs improved bioavailability, concentration at target organ, and therapeutic efficiency of docetaxel.

In the present study, we have shown that a micro-sized discoidal drug delivery system made of silk protein exhibits great potential as lung-targeted drug delivery system in the treatment of lung cancer. In particular, this study has shown the potential of DSPs to alleviate side effects and enhance the therapeutic efficacy of chemotherapeutic drugs through high biocompatibility and pH-dependent drug release. In addition, DSPs are expected to become a customized drug delivery system that can be applied to the treatment of not only lung cancer but also various lung diseases.

CRediT authorship contribution statement

Hyeyoun Cho: Writing – original draft, Methodology, Investigation, Formal analysis, Data curation. **Sanghyo Park:** Writing – original draft, Methodology, Investigation, Funding acquisition, Formal analysis, Data curation. **Jun Young Park:** Writing – original draft, Data curation. **Yoonho Hwang:** Data curation. **Won Jun Kang:** Writing – review & editing, Conceptualization. **Jaehong Key:** Writing – review & editing, Validation, Supervision, Resources, Project administration, Funding acquisition, Conceptualization.

Declaration of competing interest

The authors declare that they have no known competing financial interests or personal relationships that could have appeared to influence the work reported in this paper.

Acknowledgements

This work was supported by National Research Foundation of Korea (NRF) grants funded by the Korean government [MSIT; grant nos. RS-2024-00460405 and 2022R1F1A1069516].

Appendix A. Supplementary data

Supplementary data to this article can be found online at https://doi.org/10.1016/j.mtbio.2025.102189.

Data availability

Data will be made available on request.

References

[1] H. Sung, J. Ferlay, R.L. Siegel, M. Laversanne, I. Soerjomataram, A. Jemal, F. Bray, Global cancer statistics 2020: GLOBOCAN estimates of incidence and mortality worldwide for 36 cancers in 185 countries, CA Cancer J. Clin. 71 (3) (2021) 209–249, https://doi.org/10.3322/caac.21660.

[2] J.L. Port, B. Parashar, N. Osakwe, A. Nasar, P.C. Lee, S. Paul, B.M. Stiles, N. K. Altorki, A propensity-matched analysis of wedge resection and stereotactic body radiotherapy for early stage lung cancer, Ann. Thorac. Surg. 98 (4) (2014) 1152–1159, https://doi.org/10.1016/j.athoracsur.2014.04.128.

[3] F. Badrzadeh, M. Rahmati-Yamchi, K. Badrzadeh, A. Valizadeh, N. Zarghami, S. M. Farkhani, A. Akbarzadeh, Drug delivery and nanodetection in lung cancer, Artif. Cells, Nanomed. Biotechnol. 44 (2) (2016) 618–634, https://doi.org/10.3109/21691401.2014.975237.

[4] R.L. Siegel, A.N. Giaquinto, A. Jemal, Cancer statistics, 2024, CA Cancer J. Clin. 74 (1) (2024) 12–49, https://doi.org/10.3322/caac.21820.

[5] Y. Alduais, H. Zhang, F. Fan, J. Chen, B. Chen, Non-small cell lung cancer (NSCLC): a review of risk factors, diagnosis, and treatment, Medicine (Baltim.) 102 (8) (2023) e32899, https://doi.org/10.1097/MD.0000000000032899.

[6] S. Ashique, A. Garg, N. Mishra, N. Raina, L.C. Ming, H.S. Tulli, T. Behl, R. Rani, M. Gupta, Nano-mediated strategy for targeting and treatment of non-small cell lung cancer (NSCLC), Naunyn-Schmiedebergs Arch Pharmacol 396 (11) (2023) 2769–2792, https://doi.org/10.1007/s00210-023-02522-5.

[7] J.R. Molina, P. Yang, S.D. Cassivi, S.E. Schild, A.A. Adjei, Non-Small Cell Lung Cancer: Epidemiology, Risk Factors, Treatment, and Survivorship, Elsevier, 2008, pp. 584–594, https://doi.org/10.4065/83.5.584. Mayo clinic proceedings.

[8] P. Sharma, M. Mehta, D.S. Dhanjal, S. Kaur, G. Gupta, H. Singh, L. Thangavelu, S. Rajeshkumar, M. Tambuwala, H.A. Bakshi, D.K. Chellappan, K. Dua, S. Satija, Emerging trends in the novel drug delivery approaches for the treatment of lung cancer, Chem. Biol. Interact. 309 (2019) 108720, https://doi.org/10.1016/j.cbi.2019.06.033.

[9] J. Ahmad, S. Akhter, M. Rizwanullah, S. Amin, M. Rahman, M.Z. Ahmad, M. A. Rizvi, M.A. Kamal, F.J. Ahmad, Nanotechnology-based inhalation treatments for lung cancer: state of the art, Nanotechnol. Sci. Appl. 8 (2015) 55–66, https://doi.org/10.2147/NSA.S49052.

[10] M.A. Rahim, N. Jan, S. Khan, H. Shah, A. Madni, A. Khan, A. Jabar, S. Khan, A. Elhissi, Z. Hussain, H.C. Aziz, M. Sohail, M. Khan, H.E. Thu, Recent advancements in stimuli responsive drug delivery platforms for active and passive cancer targeting, Cancers (Basel) 13 (4) (2021) 670, https://doi.org/10.3390/cancers13040670.

[11] R. Gupta, M.M. Kadhim, A. Turki Jalil, M. Qasim Alasheqi, F. Alsaikhan, N. Khalimovna Mukhamedova, A. Alexis Ramirez-Coronel, Z. Hassan Jawhar, P. Ramaiah, M. Najafi, The interactions of docetaxel with tumor microenvironment, Int. Immunopharmacol. 119 (2023) 110214, https://doi.org/10.1016/j.intimp.2023.110214.

[12] A.R. Sa, A. Mohd Gazzali, F.A. Fisol, I.M. A, T. Parumasivam, N. Mohtar, A.W. H, Advances in nanocarriers for effective delivery of docetaxel in the treatment of lung cancer: an overview, Cancers (Basel) 13 (3) (2021) 400, https://doi.org/10.3390/cancers13030400.

[13] M. Sousa-Pimenta, L.M. Estevinho, A. Szopa, M. Basit, K. Khan, M. Armaghan, M. Ibrayeva, E. Sonmez Gurer, D. Calina, C. Hano, J. Sharifi-Rad, Chemotherapeutic properties and side-effects associated with the clinical practice of terpene alkaloids: Paclitaxel, docetaxel, and cabazitaxel, Front. Pharmacol. 14 (2023) 1157306, https://doi.org/10.3389/fphar.2023.1157306.

[14] A.M. Davies, P.N. Lara Jr., P.C. Mack, D.R. Gandara, Docetaxel in non-small cell lung cancer: a review, Expet Opin. Pharmacother. 4 (4) (2003) 553–565, https://doi.org/10.1517/14656566.4.4.553.

[15] L. Yu, S. Liu, S. Jia, F. Xu, Emerging frontiers in drug delivery with special focus on novel techniques for targeted therapies, Biomed. Pharmacother. 165 (2023) 115049, https://doi.org/10.1016/j.biopha.2023.115049.

[16] S. Adepu, S. Ramakrishna, Controlled drug delivery systems: current status and future directions, Molecules 26 (19) (2021) 5905, https://doi.org/10.3390/molecules26195905.

[17] A. Tewabe, A. Abate, M. Tamrie, A. Seyfu, E. Abdela Siraj, Targeted drug delivery - from magic bullet to nanomedicine: principles, challenges, and future perspectives, J. Multidiscip. Healthc. 14 (2021) 1711–1724, https://doi.org/10.2147/JMDH.S313968.

[18] I. Brigger, C. Dubernet, P. Couvreur, Nanoparticles in cancer therapy and diagnosis, Adv. Drug Deliv. Rev. 64 (2012) 24–36, https://doi.org/10.1016/S0169-409X(02)00044-3.

[19] A.J. Tavares, W. Poon, Y.N. Zhang, Q. Dai, R. Besla, D. Ding, B. Ouyang, A. Li, J. Chen, G. Zheng, C. Robbins, W.C.W. Chan, Effect of removing Kupffer cells on nanoparticle tumor delivery, Proc. Natl. Acad. Sci. U. S. A. 114 (51) (2017) E10871–E10880, https://doi.org/10.1073/pnas.1713390114.

[20] M.C. Arango, Y. Montoya, M.S. Peresin, J. Bustamante, C. Álvarez-López, Silk sericin as a biomaterial for tissue engineering: a review, International Journal of Polymeric Materials and Polymeric Biomaterials 70 (16) (2021) 1115–1129, https://doi.org/10.1080/00914037.2020.1785454.

[21] J. Liu, L. Shi, Y. Deng, M. Zou, B. Cai, Y. Song, Z. Wang, L. Wang, Silk sericin-based materials for biomedical applications, Biomaterials 287 (2022) 121638, https://doi.org/10.1016/j.biomaterials.2022.121638.

[22] A.S. Silva, E.C. Costa, S. Reis, C. Spencer, R.C. Calhelha, S.P. Miguel, M.P. Ribeiro, L. Barros, J.A. Vaz, P. Coutinho, Silk sericin: a promising sustainable biomaterial for biomedical and pharmaceutical applications, Polymers 14 (22) (2022) 4931, https://doi.org/10.3390/polym14224931.

[23] D.N. Rockwood, R.C. Preda, T. Yucel, X. Wang, M.L. Lovett, D.L. Kaplan, Materials fabrication from Bombyx mori silk fibroin, Nat. Protoc. 6 (10) (2011) 1612–1631, https://doi.org/10.1038/nprot.2011.379.

[24] T.P. Nguyen, Q.V. Nguyen, V.H. Nguyen, T.H. Le, V.Q.N. Huynh, D.N. Vo, Q. T. Trinh, S.Y. Kim, Q.V. Le, Silk fibroin-based biomaterials for biomedical applications: a review, Polymers 11 (12) (2019) 1933, https://doi.org/10.3390/polym11121933.

[25] S. Wang, T. Xu, Y. Yang, Z. Shao, Colloidal stability of silk fibroin nanoparticles coated with cationic polymer for effective drug delivery, ACS Appl. Mater. Interfaces 7 (38) (2015) 21254–21262, https://doi.org/10.1021/acsami.5b05335.

[26] O. Gianak, G.Z. Kyzas, V.F. Samanidou, E.A. Deliyanni, A review for the synthesis of silk fibroin nanoparticles with different techniques and their ability to be used for drug delivery, Curr. Anal. Chem. 15 (4) (2019) 339–348, https://doi.org/10.2174/1573411014666180917110650.

[27] S.Y. Yu, W.H. Yang, S. Chen, M.J. Chen, Y.Z. Liu, Z.Z. Shao, X. Chen, Floxuridine-loaded silk fibroin nanospheres, RSC Adv. 4 (35) (2014) 18171–18177, https://doi.org/10.1039/C4RA02113D.

[28] M.S. Zafar, K.H. Al-Samadani, Potential use of natural silk for bio-dental applications, J Taibah Univ Sci 9 (3) (2014) 171–177, https://doi.org/10.1016/j.jtumed.2014.01.003.

[29] Z. Jiao, Y. Song, Y. Jin, C. Zhang, D. Peng, Z. Chen, P. Chang, S.C. Kundu, G. Wang, Z. Wang, L. Wang, In vivo characterizations of the immune properties of sericin: an ancient material with emerging value in biomedical applications, Macromol. Biosci. 17 (12) (2017) 1700229, https://doi.org/10.1002/mabi.201700229.

[30] E.M. El-Fakharany, G.M. Abu-Elreesh, E.A. Kamoun, S. Zaki, D.A. Abd-El-Haleem, In vitro assessment of the bioactivities of sericin protein extracted from a bacterial silk-like biopolymer, RSC Adv. 10 (9) (2020) 5098–5107, https://doi.org/10.1039/C9RA09419A.

[31] J.P. Kumar, B.B. Mandal, Silk sericin induced pro-oxidative stress leads to apoptosis in human cancer cells, Food Chem. Toxicol. 123 (2019) 275–287, https://doi.org/10.1016/j.fct.2018.10.063.

[32] S. Mumtaz, S. Ali, A. Pervaiz, M.Z. Qureshi, K. Kanwal, T. Saleem, Apoptotic and antiproliferative effects of silk protein sericin conjugated-AgNO3 nanoparticles in human breast cancer cells, Saudi J. Biol. Sci. 30 (2) (2023) 103551, https://doi.org/10.1016/j.sjbs.2022.103551.

[33] S.A. Matthew, F.P. Seib, The dawning era of anticancer nanomedicines: from first principles to application of silk nanoparticles, Adv. Therapeut. 8 (1) (2025) 2400130, https://doi.org/10.1002/adtp.202400130.

[34] N. Roamcharern, S.A. Matthew, D.J. Brady, J.A. Parkinson, Z. Rattray, F.P. Seib, Biomimetic silk nanoparticle manufacture: calcium ion-mediated assembly, ACS Biomater. Sci. Eng. 11 (3) (2025) 1847–1856, https://doi.org/10.1021/acsbiomaterials.4c02175.

[35] S. Shaidani, C. Jacobus, J.K. Sahoo, K. Harrington, H. Johnson, O. Foster, S. Cui, O. Hasturk, T. Falcucci, Y. Chen, Silk nanoparticle synthesis: tuning size, dispersity, and surface chemistry for drug delivery, ACS Appl. Nano Mater. 6 (20) (2023) 18967–18977, https://doi.org/10.1021/acsanm.3c03451.

[36] L. Züge, V. Silva, F. Hamerski, M. Ribani, M. Gimenes, A. Scheer, Emulsifying properties of sericin obtained from hot water degumming process, J. Food Process. Eng. 40 (1) (2017) e12267, https://doi.org/10.1111/jfpe.12267.

[37] T. Välisalmi, H. Bettahar, Q. Zhou, M.B. Linder, Pulling and analyzing silk fibers from aqueous solution using a robotic device, Int. J. Biol. Macromol. 250 (2023) 126161, https://doi.org/10.1016/j.ijbiomac.2023.126161.

[38] Y.Q. Zhang, Applications of natural silk protein sericin in biomaterials, Biotechnol. Adv. 20 (2) (2002) 91–100, https://doi.org/10.1016/S0734-9750(02)00003-4.

[39] C.S. Ki, J.W. Kim, H.J. Oh, K.H. Lee, Y.H. Park, The effect of residual silk sericin on the structure and mechanical property of regenerated silk filament, Int. J. Biol. Macromol. 41 (3) (2007) 346–353, https://doi.org/10.1016/j.ijbiomac.2007.05.005.

[40] D.Y. Lee, S.W. Lee, S.K. Kim, M. Lee, H.W. Chang, H.T. Moon, Y. Byun, S.Y. Kim, Antiangiogenic activity of orally absorbable heparin derivative in different types of cancer cells, Pharm. Res. 26 (12) (2009) 2667–2676, https://doi.org/10.1007/s11095-009-9989-9.

[41] D.D. Sominski, P. Rafferty, K. Brosnan, A. Volk, M. Walker, D. Capaldi, E. Emmell, K. Johnson, D. Weinstock, Development of a squamous cell carcinoma mouse model for immunotoxicity testing, J. Immunot. 13 (2) (2016) 226–234, https://doi.org/10.3109/1547691X.2015.1045105.

[42] S. Park, J.Y. Park, J.H. Nahm, G. Kim, Y. Cho, W. Kang, J. Key, Systemic delivery of nintedanib using PLGA-based discoidal polymeric particles for idiopathic pulmonary fibrosis treatment, Mater. Today Chem. 26 (2022) 101181, https://doi.org/10.1016/j.mtchem.2022.101181.

[43] M. Ma, Y. Hao, N. Liu, Z. Yin, L. Wang, X. Liang, X. Zhang, A novel lipid-based nanomicelle of docetaxel: evaluation of antitumor activity and biodistribution, Int. J. Nanomed. 7 (2012) 3389–3398, https://doi.org/10.2147/IJN.S29827.

[44] A. Gaviria, N. Jaramillo-Quiceno, A. Motta, A. Restrepo-Osorio, Silk wastes and autoclaved degumming as an alternative for a sustainable silk process, Sci. Rep. 13 (1) (2023) 15296, https://doi.org/10.1038/s41598-023-41762-6.

[45] J. Saha, M.I. Mondal, M.K. Sheikh, M.A. Habib, Extraction, structural and functional properties of silk sericin biopolymer from Bombyx mori silk cocoon waste, J. Textil. Sci. Eng. 9 (1) (2019) 1000390, https://doi.org/10.4172/2165-8064.1000390.

[46] S. Du, J. Zhang, W.T. Zhou, Q.X. Li, G.W. Greene, H.J. Zhu, J.L. Li, X.G. Wang, Interactions between fibroin and sericin proteins from Antheraea pernyi and Bombyx mori silk fibers, J. Colloid Interface Sci. 478 (2016) 316–323, https://doi.org/10.1016/j.jcis.2016.06.030.

[47] S. Chen, X. Feng, X. Li, M. Liu, W. Gao, Q. Miao, H. Wu, Microparticles of sericin-dextran conjugate for improving the solubility of antiviral drug, J. Funct. Biomater. 14 (6) (2023) 292, https://doi.org/10.3390/jfb14060292.
[48] V. Singh, D. Srivastava, P. Pandey, M. Kumar, S. Yadav, D. Kumar, Characterization, antibacterial and anticancer study of silk fibroin hydrogel, J. Drug Deliv. Therapeut. 13 (2) (2023), https://doi.org/10.22270/jddt.v13i2.5733.
[49] A. Hekmat, H. Attar, A.A. Seyf Kordi, M. Iman, M.R. Jaafari, New oral formulation and in vitro evaluation of docetaxel-loaded nanomicelles, Molecules 21 (9) (2016) 1265, https://doi.org/10.3390/molecules21091265.
[50] K.N. Clayton, J.W. Salameh, S.T. Wereley, T.L. Kinzer-Ursem, Physical characterization of nanoparticle size and surface modification using particle scattering diffusometry, Biomicrofluidics 10 (5) (2016) 054107, https://doi.org/10.1063/1.4962992.
[51] G. Hao, Z.P. Xu, L. Li, Manipulating extracellular tumour pH: an effective target for cancer therapy, RSC Adv. 8 (39) (2018) 22182–22192, https://doi.org/10.1039/C8RA02095G.
[52] N.V. Di Russo, D.A. Estrin, M.A. Marti, A.E. Roitberg, pH-Dependent conformational changes in proteins and their effect on experimental pK(a)s: the case of Nitrophorin 4, PLoS Comput. Biol. 8 (11) (2012) e1002761, https://doi.org/10.1371/journal.pcbi.1002761.
[53] H.J. Jin, J. Park, V. Karageorgiou, U.J. Kim, R. Valluzzi, D.L. Kaplan, Water-stable silk films with reduced β-sheet content, Adv. Funct. Mater. 15 (8) (2005) 1241–1247, https://doi.org/10.1002/adfm.200400405.
[54] S.U.D. Wani, M.I. Zargar, M.H. Masoodi, S. Alshehri, P. Alam, M.M. Ghoneim, A. Alshlowi, H.G. Shivakumar, M. Ali, F. Shakeel, Silk fibroin as an efficient biomaterial for drug delivery, gene therapy, and wound healing, Int. J. Mol. Sci. 23 (22) (2022) 14421, https://doi.org/10.3390/ijms232214421.
[55] E. Mustafa, N.A. Rajab, Preparation and in-vitro evaluation of Paclitaxel-loaded sericin nanoparticles planned for pulmonary drug delivery system, ACTA Pharmaceutica Sciencia 63(2). https://doi.org/10.23893/1307-2080.APS6328.
[56] D.T. Pham, D.X.T. Nguyen, N.Y. Nguyen, T.T.L. Nguyen, T.Q.C. Nguyen, A.V.T. Tu, N.H. Nguyen, B.T.P. Thuy, Development of pH-responsive Eudragit S100-functionalized silk fibroin nanoparticles as a prospective drug delivery system, PLoS One 19 (5) (2024) e0303177, https://doi.org/10.1371/journal.pone.0303177.
[57] S. Ratanabunyong, J. Siriwaseree, P. Wanaragthai, S. Krobthong, Y. Yingchutrakul, B. Kuaprasert, K. Choowongkomon, P. Aramwit, Exploring the apoptotic effects of sericin on HCT116 cells through comprehensive nanostring transcriptomics and proteomics analysis, Sci. Rep. 14 (1) (2024) 2366, https://doi.org/10.1038/s41598-024-52789-8.
[58] K.S. Oh, K. Kim, B.D. Yoon, H.J. Lee, D.Y. Park, E.Y. Kim, K. Lee, J.H. Seo, S.H. Yuk, Docetaxel-loaded multilayer nanoparticles with nanodroplets for cancer therapy, Int. J. Nanomed. 11 (2016) 1077–1087, https://doi.org/10.2147/IJN.S100170.
[59] R. Chen, S. Ni, W. Chen, M. Liu, J. Feng, K. Hu, Improved anti-triple negative breast cancer effects of docetaxel by RGD-modified lipid-core micelles, Int. J. Nanomed. 16 (2021) 5265–5279, https://doi.org/10.2147/IJN.S313166.
[60] Á.A. Cortés, L.C. Urquizu, J.H. Cubero, Adjuvant chemotherapy in non-small cell lung cancer: state-of-the-art, Transl. Lung Cancer Res. 4 (2) (2015) 191, https://doi.org/10.3978/j.issn.2218-6751.2014.06.01.
[61] J.-P. Sculier, Anticancer treatment for advanced non-small cell lung cancer, Breathe 8 (2) (2011) 124–133, https://doi.org/10.1183/20734735.005011.
[62] M.A. Gubens, H.A. Wakelee, Docetaxel in the treatment of non-small cell lung carcinoma: an update and analysis, Lung Cancer 1 (2010) 63–76, https://doi.org/10.2147/LCTT.S6499.
[63] Q. Lu, B. Zhang, M. Li, B. Zuo, D.L. Kaplan, Y. Huang, H. Zhu, Degradation mechanism and control of silk fibroin, Biomacromolecules 12 (4) (2011) 1080–1086, https://doi.org/10.1021/bm101422j.
[64] X. Wang, T. Yucel, Q. Lu, X. Hu, D.L. Kaplan, Silk nanospheres and microspheres from silk/pva blend films for drug delivery, Biomaterials 31 (6) (2010) 1025–1035, https://doi.org/10.1016/j.biomaterials.2009.11.002.
[65] L. Niu, S. Yang, X. Zhao, X. Liu, L. Si, M. Wei, L. Liu, L. Cheng, Y. Qiao, Z. Chen, Sericin inhibits MDA-MB-468 cell proliferation via the PI3K/Akt pathway in triple-negative breast cancer, Mol. Med. Rep. 23 (2) (2021), https://doi.org/10.3892/mmr.2020.11779, 1-1.
[66] S.E. Diab, N.A. Tayea, B.H. Elwakil, S.S. Elshewemi, A. Gad, S.A. Abdulmalek, D. A. Ghareeb, Z.A. Olama, In vitro and in vivo anti-colorectal cancer effect of the newly synthesized sericin/propolis/fluorouracil nanoplatform through modulation of PI3K/AKT/mTOR pathway, Sci. Rep. 14 (1) (2024) 2433, https://doi.org/10.1038/s41598-024-52722-z.
[67] S. Park, H. Park, C. Park, W.S. Yun, S. Hwang, H.Y. Yoon, I.C. Kwon, K. Kim, J. Key, Improved survival rate and minimal side effects of doxorubicin for lung metastasis using engineered discoidal polymeric particles, Biomater. Sci. 10 (15) (2022) 4335–4344, https://doi.org/10.1039/d2bm00718e.
[68] P. Decuzzi, B. Godin, T. Tanaka, S.Y. Lee, C. Chiappini, X. Liu, M. Ferrari, Size and shape effects in the biodistribution of intravascularly injected particles, J. Contr. Release 141 (3) (2010) 320–327, https://doi.org/10.1016/j.jconrel.2009.10.014.
[69] J.A. Champion, A. Walker, S. Mitragotri, Role of particle size in phagocytosis of polymeric microspheres, Pharm. Res. 25 (8) (2008) 1815–1821, https://doi.org/10.1007/s11095-008-9562-y.
[70] M.W. Helmy, M.H. Youssef, I. Yamari, A. Amr, F.I. Moussa, A. El Wakil, S. Chtita, L. M. El-Samad, M.A. Hassan, Repurposing of sericin combined with dactolisib or vitamin D to combat non-small lung cancer cells through computational and biological investigations, Sci. Rep. 14 (1) (2024) 27034, https://doi.org/10.1038/s41598-024-76947-0.
[71] X. Zhang, J. Shao, X. Li, L. Cui, Z. Tan, Docetaxel promotes cell apoptosis and decreases SOX2 expression in CD133-expressing hepatocellular carcinoma stem cells by suppressing the PI3K/AKT signaling pathway, Oncol. Rep. 41 (2) (2019) 1067–1074, https://doi.org/10.3892/or.2018.6891.
[72] M.J. Sanaei, S. Razi, A. Pourbagheri-Sigaroodi, D. Bashash, The PI3K/Akt/mTOR pathway in lung cancer; oncogenic alterations, therapeutic opportunities, challenges, and a glance at the application of nanoparticles, Transl. Oncol. 18 (2022) 101364, https://doi.org/10.1016/j.tranon.2022.101364.
[73] E. Blanco, H. Shen, M. Ferrari, Principles of nanoparticle design for overcoming biological barriers to drug delivery, Nat. Biotechnol. 33 (9) (2015) 941–951, https://doi.org/10.1038/nbt.3330.
[74] W. Choi, H. Cho, G. Kim, I. Youn, J. Key, S. Han, Targeted thrombolysis by magnetoacoustic particles in photothrombotic stroke model, Biomater. Res. 26 (1) (2022) 58, https://doi.org/10.1186/s40824-022-00298-y.
[75] J.Y. Park, S. Park, T.S. Lee, Y.H. Hwang, J.Y. Kim, W.J. Kang, J. Key, Biodegradable micro-sized discoidal polymeric particles for lung-targeted delivery system, Biomaterials 218 (2019) 119331, https://doi.org/10.1016/j.biomaterials.2019.119331.